

PHYSICAL REVIEW A

ATOMIC, MOLECULAR, AND OPTICAL PHYSICS

THIRD SERIES, VOLUME 49, NUMBER 4

APRIL 1994

RAPID COMMUNICATIONS

The Rapid Communications section is intended for the accelerated publication of important new results. Since manuscripts submitted to this section are given priority treatment both in the editorial office and in production, authors should explain in their submittal letter why the work justifies this special handling. A Rapid Communication should be no longer than 4 printed pages and must be accompanied by an abstract. Page proofs are sent to authors.

Talbot-vonLau atom interferometry with cold slow potassium

John F. Clauser and Shifang Li

Physics Department, University of California–Berkeley, Berkeley, California 94720

(Received 30 August 1993)

A dc hot thermal and an ac-modulated cold slow potassium beam copropagate and pass through an atom de Broglie-wave interferometer, consisting of a sequence of three microfabricated diffraction gratings. Talbot-vonLau interference fringes are formed and sensed by measuring transmission with a hot wire as a function of grating position. The hot beam produces diffraction-limited shadow Moiré fringes, while the longer de Broglie wavelength slow beam produces interference fringes with high visibility at the fifth and sixth spatial harmonics of the shadow Moiré fringes.

PACS number(s): 03.75.Dg, 32.80.-t, 42.50.-p, 07.60.Ly

Following suggestions by Altshuler and Frantz [1], Dubetskii *et al.* [2], and Clauser [3], there is recent interest in de Broglie-wave interference exhibited by the propagation of whole neutral atoms [4]. Kieth *et al.* [5] used gratings in a split beam-envelope (SBE) geometry to split a fast atomic beam into several beams, to reconverge and superpose two of the beams to form sinusoidal fringes, and finally to mask the fringes to allow their detection. In this Rapid Communication we report the operation of an atom interferometer that also uses gratings but does not split the beam envelope. Instead, it forms interference fringes via the generalized Talbot-vonLau (TvL) effect [6]. TvL interferometry has two major advantages over SBE interferometry. First, to prevent overlap of diffraction orders, SBE interferometry requires narrow input beam collimation which severely restricts its throughput. TvL interferometry accepts a very wide beam solid angle. Although our source brightness for cold slow atoms is 2500 times weaker than that of Ref. [5], the peak-to-peak amplitude of our interference signal is about 3000 times stronger. Second, the required diffraction grating period scales with the square root of the de Broglie wavelength rather than linearly. Thus, although the de Broglie wavelength in our interferometer is

only 3.2 times longer than that of Ref. [5], our middle grating's period is 20.5 times larger. Grating fabrication is thus easier.

Our apparatus is diagrammed in Fig. 1. A vacuum chamber with a vertical orientation is divided in two by a differential pumping (DP) slit. Background potassium vapor is limited by liquid-nitrogen (LN) cooled baffles. In the lower chamber (at 10^{-8} Torr) we generate copropagating dc thermal and ac-modulated cold slow potassium beams [7]. Thermal potassium atoms effuse from a $200\ \mu\text{m} \times 5\ \text{mm}$ knife-edge slit in the top of a 450-K copper oven, pass through a $300\ \mu\text{m} \times 8\ \text{mm}$ collimating slit, a cold baffle, the DP slit, and into the upper chamber (at 10^{-9} Torr), where they pass through the interferometer to a detector. The oven slit is offset from the interferometer axis so that only one wing of the collimated thermal beam (produced by scattering near the oven slit) passes through the interferometer to the detector. Cold slow atoms are velocity selected by using laser light to deflect them out of the offset parent thermal beam onto the interferometer axis. The laser beam crosses the atomic beam immediately below the collimating slit at 20° from the comoving parallel. The parallel component of the laser's incidence provides Doppler velocity selection

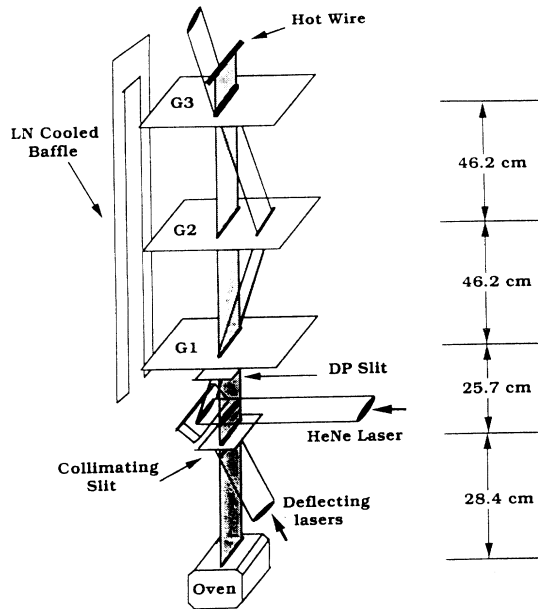


FIG. 1. Geometry of the experimental apparatus. LN denotes liquid nitrogen.

of atoms from the low-velocity portion of the parent beam's thermal distribution, while the perpendicular component provides momentum transfer for deflection. The small deflection angle (≈ 0.5 mrad) requires scattering of only about seven photons, so that perpendicular heating of the slow atoms is minimal and a source brightness of about 4×10^{15} atoms/cm² sr⁻¹ sec⁻¹ is achieved for 182 m/sec atoms.

The ribbon-shaped laser beam has two frequency components (deflecting and repumping) each produced by a separate single-mode diode laser at 766 nm. The components are separated by 437 MHz, and each has a bandwidth of about 15 MHz (estimated by observing their heterodyne with a fast photodiode and a rf spectrum analyzer). To calibrate the laser tunings, we redirect the laser beam to cross the atomic beam at perpendicular incidence. Then, when either laser alone is tuned to a Doppler-free hyperfine resonance, deflection of the whole beam produces a change in the atomic beam current [7].

Transmitted atomic current is detected via surface ionization on a rhenium hot wire. The resulting positive-ion current is electrostatically focused onto an electron multiplier, whose analog anode current is further amplified with a 5-msec time constant. To allow us to distinguish the two beam components, the deflecting laser is ac modulated. The 320-msec modulation period is divided into six parts with the sequence, STAB-ON-OFF-STAB-OFF-ON. During each 80-ms STAB period, the laser wavelengths are locked to the potassium *D2* resonance line of an absorption cell. During the ON and OFF periods (40 ms each) the lasers are unlocked and tuned to select atoms at 182 m/sec. During each OFF period the deflecting laser light is blocked by a liquid-crystal shutter. The average dc hot-wire signal represents that due to the thermal velocity component of the atomic current. The weak ac component of the current is synchronously detected by an "up-down boxcar integrator" (two poles,

with 1.0- and 3.7-sec integration times respectively). The integration is gated off during the laser stabilization period. During each ON period, the current is integrated with a positive sign, while during each OFF period, integration occurs with a negative sign. The integration gates include compensation for the amplifier response and atomic transit times. The dc component cancels, and the above sequence minimizes cross talk from the dc signal's first time derivative.

Use of circular polarization and two optical frequencies pumps atoms out of the $4s^2S_{1/2}(F=1)$ level and allows cycling of the $^{39}\text{K } 4s^2S_{1/2}(F=2) \rightarrow 4p^2P_{3/2}(F=3)$ deflecting transition. Since high-velocity $F=2$ atoms excited by the unmodulated repumping light can contribute no ac signal, but a fivefold decrease in the ac signal occurs when no repumping light is applied, we conclude that low-velocity cycling atoms dominate the ac signal, and that the velocity bandwidth of the cold slow atoms is set by the deflecting laser's bandwidth and is not significantly broadened by upper-state hyperfine structure. Narrower resonance widths of cycling transitions (relative to noncycling) observed during the perpendicular incidence wavelength calibrations support this assertion.

Figure 2(a) shows two possible computer-simulated velocity profiles (both well within our uncertainty) for the ac slow beam produced when the lasers are tuned to deflect $F=2$ atoms at 182 m/sec. With very weak excitation by the laser's Lorentzian wings, a weak broad ac phase-reversed background component is produced by deflecting (and heating) atoms in the transmitted wing of the offset parent dc beam's wing farther away from the detector. An in-phase velocity component is produced only by stronger excitation at line center when atoms are deflected from the center of the offset parent beam all of the way onto the interferometer's axis. The maximum transmitted ac current is roughly 4×10^5 atoms/sec at 182 m/sec. The dc current is about 130 times stronger, and the signal-to-noise ratio of the ac signal is limited by the shot noise of the dc current and/or low electron mul-

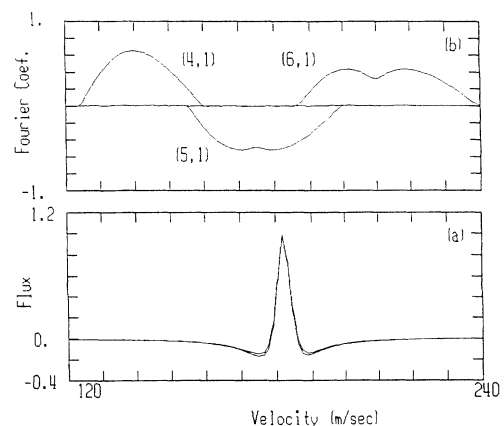


FIG. 2. (a) Two possible velocity profiles for our source, assuming a parallel velocity spread of about 10–12 m/sec. Positive and negative signs correspond to in-phase and phase-reversed ac signal levels. (b) Fourth, fifth, and sixth spatial harmonic content of the calculated fringe pattern at the respective $(m,n)=(4,1)$, $(5,1)$, and $(6,1)$ resonances.

tiplier secondary electron emission.

The interferometer consists of a sequence of three parallel planes, each containing a rectangular vacuum-slit transmission grating. The spacings between the grating planes are $R_1=R_2=46.2$ cm. The gratings are micro-fabricated from $1\text{-}\mu\text{m}$ -thick silicon-nitride membranes supported by silicon frames, with parallel slits etched through the membranes. Grating fabrication employed conventional optical lithography and etching techniques. The first and third gratings have the same period, $a_1=a_3=16.2\text{ }\mu\text{m}$, and have 22 and 76 slits, respectively. The middle grating has 111 slits, with a period, $a_2=8.1\text{ }\mu\text{m}$. All three are 8.5 mm long and have an average open fraction of about $s/a=1/8$, where s is the slit width. The gratings are positioned through bellows via optical translation stages, mounted on a rigid framework surrounding the vacuum chamber. The framework and chamber are vibrationally isolated from the floor, and are stationary relative to an inertial frame to a fraction of a micrometer during the transit time of a low-velocity atom through the interferometer. Grating rotational alignment uses a HeNe laser that is collimated by a cylindrical telescope to form a "bow-tie" ribbon focus. The laser beam forms a SBE optical interferometer using all three gratings. The laser beam is split by the first grating. At the middle grating plane it passes through both the middle grating, and a fourth additional identical grating, displaced to one side. The split beams reconverge and form magnified optical Moiré fringes with the third atom grating. The bow tie's focal vertex may be positioned on any one grating's plane. Correct alignment is sensed when optical fringe parallelism is independent of the telescope's focus.

For an interferometer with the above geometry Clauser and Reinsch [6] pointed out that de Broglie-wave fringes will be formed on and masked by the third grating via the generalized Talbot-vonLau effect. Fringes are sensed by monitoring the variation of the transmission in response to slowly scanning the middle grating's position (with a piezoelectric translator). An interfering path set within the beam envelope consists of nested diamonds, starting at one source slit in the first grating and forming an interference pattern on the third. Throughput and solid angle acceptance are enhanced by incoherent addition of the current from many source slits on the first grating, each providing many such nested diamonds at all possible skew angles between the first and second gratings' slits.

The fringe pattern (and transmitted current) contains various spatial harmonics of the geometric shadow period. Each harmonic will be resonant in the interferometer at a different atomic velocity. Figure 2(b) shows the calculated amplitudes for the fourth, fifth, and sixth harmonic components of a Fourier decomposition of the pattern as a function of atomic velocity. A resonance for the m th harmonic occurs at $\lambda_{dB}/\lambda_{TR}=n/m$ when m and n approximate small integers. Here, λ_{dB} is the atoms' de Broglie wavelength, $\lambda_{TR}\equiv a_2^2/\rho$ is the interferometer's Talbot-Rayleigh wavelength, and $\rho\equiv R_1R_2/(R_1+R_2)$ is the interferometer's reduced length. For our geometry the associated resonant atomic velocity is $(m/n)v_{TR}$, where $v_{TR}\approx 35$ m/sec. Phase re-

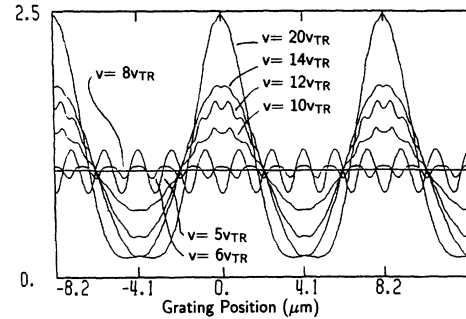


FIG. 3. Calculated normalized interferometer transmission as a function of and grating displacement, for various atomic velocities, 175, 210, 280, 350, 419, 489, and 699 m/sec, corresponding to 5, 6, 8, 10, 12, 14, and 20 times v_{TR} , respectively.

versal of the $(m,n)=(5,1)$ resonance (fifth harmonic) is a consequence of the fact that the product, mn , is odd.

Figure 3 shows for various atomic velocities the calculated interferometer transmission as a function of grating displacement, averaged over the finite slit widths of the first and third gratings. At velocities above $(a_2/s_2)v_{TR}\approx 8v_{TR}\approx 278$ m/sec, the oscillatory fringe structures give way to the $(n\rightarrow 0)$ geometric shadow. The calculated ac and dc signals at any grating position are given by a weighted integration of the transmission over atomic velocity. For the ac signal, a weighting by the velocity profile of Fig. 2(a) samples a narrow range of the velocities where high-frequency oscillatory fringe structures occur. The peak of our thermal distribution occurs at about 540 m/sec, and a thermally distributed weighting yields a diffraction-limited geometric Moiré for the dc fringe pattern.

Figure 4(a) shows the measured (solid) and calculated (dashed)

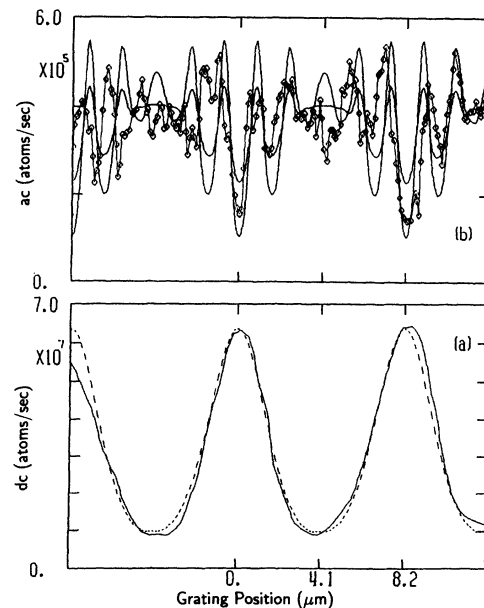


FIG. 4. (a) Measured (solid line) and calculated (dashed line) dc signal as a function of grating relative displacement. Zero level corresponds to the laser-blocked condition. (b) Simultaneously measured ac signal (diamond points) and calculated ac signals (with the vertical offsets suppressed), for the different assumed velocity distributions of Fig. 2(a).

(dashed) dc signal as a function of grating position, while Fig. 4(b) shows the simultaneously measured ac signal in response to a single scan of the middle grating. Each data point represents about a 4-sec integration. The grating displacement axis suffers from a nonlinear distortion for negative values, evident in both the ac and dc signals. It is due to start-up hysteresis in our piezoelectric translator. Despite this distortion a fifth spatial-harmonic component is clearly evident in the ac signal. Since the laser tuning selects atoms near the $(m,n)=(5,1)$ resonance, this harmonic is expected to dominate. However, given the v^3 weighting of atoms in the parent beam, the phase-reversed high-velocity broad Lorentzian wing of the profile contributes a significant sixth harmonic at opposite phase that enhances end fringes and washes out central fringes. Figure 4(b) also shows the associated calculated ac fringe patterns for the two assumed incident ac velocity profiles of Fig. 2(a). A small change in the excitation spectrum difference has a strong effect on the shape of the pattern. Had we instead assumed a broad nonreversed velocity profile in our simulation, the strong peaks would be shifted by half a dc fringe period. It also has a significant effect on the vertical offset of the pattern [suppressed in Fig. 4(c)], since excitations of the fifth and sixth (modest visibility) harmonics are of opposite phase. Cancellation of the associated opposite vertical offset thus enhances the apparent ac fringe visibility. Thus, although the observed ac fringe visibility is about 80% referenced to the blocked-laser ac signal level, that of each velocity component is probably lower. Calculation assuming various v/a values indicates that the asymmetry and finite visibility of the dc fringe pattern are due

dominantly to quantum-mechanical diffraction by the second grating and more weakly to geometrical averaging by the first and third gratings. By monitoring the dc fringe pattern's asymmetry and visibility over time, we establish that a buildup of potassium slowly narrows the slit openings, while baking widens them.

Runs with the lasers blocked indicate negligible cross talk between the ac and dc signals. Phase shifts from gravity and from stray magnetic and electric fields are negligible. A strong Sagnac phase shift of the dc Moiré fringe signal is immediately evident whenever the chamber is touched, even lightly. The ac fringe shape is quite sensitive to laser tuning. ac fringe patterns for smaller harmonic number, m , are observed at lower velocities, but given the v^3 dependence of the source current, these have poorer signal-to-noise ratio. If the chamber's vibration isolation is defeated, then a reduction in dc fringe visibility and an absence of ac fringes results. Misaligned gratings produce no ac fringes and sinusoidal diminished visibility dc fringes. No ac fringes are produced when the LN cooled baffles are warm, suggesting that collisions with background potassium and/or water then occur.

This work was supported by ONR Grant No. N00014-90-J-1475 and the firm J. F. Clauser & Assoc., Walnut Creek, CA. The authors wish to thank M. Reinsch, G. Garfein, and the staff and students at the UC Berkeley Microstructures Laboratory for their assistance in this work.

-
- [1] S. Altschuler and L. M. Frantz, US Patent No. 3 761 721.
 [2] B. Ya. Dubetskii *et al.*, *Pis'ma, Zh. Eksp. Teor. Fiz.* **39**, 531 (1984) [*JETP Lett.* **39**, 649 (1984)].
 [3] J. F. Clauser, *Physica B* **151**, 262 (1988); U.S. Patents No. 4 874 942 and No. 4 992 656.
 [4] O. Carnal and J. Mlynek, *Phys. Rev. Lett.* **66**, 2689 (1991); F. Shimizu *et al.*, *Phys. Rev. A* **46**, R17 (1992); M. Kase-

- vich and S. Chu, *Phys. Rev. Lett.* **67**, 181 (1991); U. Sterr *et al.*, *Appl. Phys. Lett.* **B 54**, 341 (1992); F. Riehle *et al.*, *Phys. Rev. Lett.* **67**, 177 (1991).
 [5] D. W. Keith *et al.*, *Phys. Rev. Lett.* **66**, 2693 (1991).
 [6] J. F. Clauser and M. W. Reinsch, *Appl. Phys. B* **54**, 380 (1992), and references therein.
 [7] S. Li and J. F. Clauser, *Phys. Rev. A* **49**, 2702 (1994).

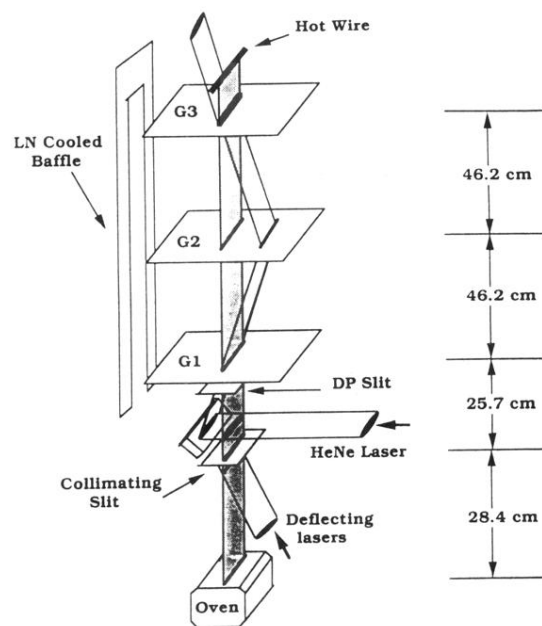


FIG. 1. Geometry of the experimental apparatus. LN denotes liquid nitrogen.